INSTITUTE OF PHYSICS PUBLISHING NONLINEARITY

Nonlinearity **19** (2006) 531–552 doi:10.1088/0951-7715/19/3/001

On multi-parametric bifurcations in a scalar piecewise-linear map

Viktor Avrutin and Michael Schanz

Institute of Parallel and Distributed Systems (IPVS), University of Stuttgart, Universitätstrasse 38, D-70569 Stuttgart, Germany

E-mail: Viktor.Avrutin@informatik.uni-stuttgart.de and Michael.Schanz@informatik.uni-stuttgart.de

Received 4 May 2005, in final form 23 November 2005
Published 13 January 2006
Online at stacks.iop.org/Non/19/531

Recommended by B Eckhardt

Abstract

In this work a one-dimensional piecewise-linear map is considered. The areas in the parameter space corresponding to specific periodic orbits are determined. Based on these results it is shown that the structure of the 2D and 3D parameter spaces can be simply described using the concept of multi-parametric bifurcations. It is demonstrated that an infinite number of two-parametric bifurcation lines starts at the origin of the 3D parameter space. Along each of these lines an infinite number of bifurcation planes starts, whereas the origin represents a three-parametric bifurcation.

PACS numbers: 05.45.−a, 05.45.Ac, 82.40.Bj, 95.10.Fh

1. Introduction

Dynamical systems with a piecewise defined system function are a very important subject of interest from a theoretical and application point of view and have been intensively investigated in the past years. They occur naturally in many scientific disciplines. For instance, in electronics adequate models of some power circuits (such as dc/dc converters) are represented by dynamical systems with piecewise-smooth system functions (both continuous and discontinuous) [1–14]. Additionally, the models of some mechanical systems such as impact or stick–slip oscillators are represented by dynamical systems with piecewise-smooth discontinuous system functions (see, e.g., [15–25]). Furthermore, piecewise-smooth and discontinuous maps occur naturally as Poincaré return maps of dynamical systems continuous in time, which exhibit chaotic dynamics [26, 27]. In this case, the discontinuity of the system function is based on the stretching, squeezing and folding phenomena, which are inherent to chaotic attractors. One of the most important characteristic properties of dynamical systems with piecewise-smooth system functions is their ability to undergo border-collision

bifurcations. These bifurcations, occurring at the border between partitions in the state space, were intensively studied in many works, for instance, in [28–50, 5, 7, 10, 21]. Recently, several types of border collision related bifurcations were found, such as corner collision, sliding bifurcations and dangerous border collision bifurcations [42, 49, 51, 52]. Overviews about bifurcations in piecewise-smooth dynamical systems and related phenomena can be found, for instance, in [13, 25, 49, 50, 53]. Multi-parametric (or co-dimension $n > 1$) bifurcations are bifurcations which can be observed only under simultaneous variation of some number $n > 1$ of system parameters [54–59]. These bifurcations are, in general, a challenging topic and are currently the main focus of many publications in the field of nonlinear dynamics [48, 50, 60–62]. As in many of these fields, they also lead in the case of piecewise-smooth systems to a large number of open questions.

In this work we present some results related to this topic obtained by the investigation of a piecewise-linear map. There are mainly three reasons for the investigation of a piecewise-linear map.

- In this case many results can be obtained by pure analytical calculations.
- Meanwhile it is known that piecewise-linear maps represent some kind of normal forms for some border-collision bifurcations [63].
- The basic principles and mechanisms leading to many border-collision related phenomena can be studied without loss of generality using piecewise-linear systems. Fortunately, in this case it is possible to separate the phenomena induced by interactions with borders in the state space from phenomena based on other nonlinearities.

For these reasons, piecewise-linear maps represent an important framework for the investigation of piecewise-smooth systems. Therefore, piecewise-linear maps have been used since early works on this field [32, 35, 64]. Later, they were intensively investigated by many authors (see for instance [7, 45, 65–70]). Some well-known scalar dynamical systems belong to this class, such as the tent map and the Bernoulli map [71]. Examples of two-dimensional piecewise-linear maps are the Lozi map [72], the Gingerbreadman map [73] and Smale's horseshoe map [74]. The system discussed in our work is similar to the models used in [75] for the investigation of the simplified Oregonator ([76–78]).

Our paper is organized as follows. In section 2, the investigated dynamical system is defined and some of the notation used is introduced. Then in section 3, the characteristic areas in the parameter space are identified and the region of the parameter space is specified, which we investigate in more detail. In order to get an overview of the dynamic behaviour of the investigated system, some numeric results are presented in this section as well. After that, in section 4 the mechanism leading to the existence of stable periodic orbits in the investigated system is briefly discussed and some analytical results are obtained. Based on these results in section 5 the bifurcation structures in the 2D parameter space depending on the third parameter are described. Section 6 unifies these results and describes the overall structure of the 3D parameter space. In section 7 the presented results are considered in a more general context and the concepts of two- and multi-parametric bifurcations are discussed. These concepts lead us to a simple explanation of the complex bifurcation structures in the 3D parameter space of the investigated system.

2. Investigated dynamical system

We consider a 1D map with a piecewise-linear system function, defined by

$$x_{n+1} = \begin{cases} f_l(x_n) = bx_n + c & \text{if } x_n < 0, \\ f_r(x_n) = x_n - a & \text{if } x_n \geqslant 0, \end{cases} \tag{1}$$

Table 1. Characteristic areas in the 3D parameter space of the considered piecewise-linear map and the corresponding asymptotic dynamics.

Area in the 3D parameter space	Asymptotic behaviour
$\Pi_1 = \{(a,b,c)\|a<0, b>1, c<0\}$	All orbits diverge towards $-\infty$ or ∞
$\Pi_2 = \{(a,b,c)\|a<0, \|b\|<1, c<0\}$	Point x^* is a stable fixed point. Orbits started at $x_0 < 0$ converge to x^*, other orbits diverge towards ∞
$\Pi_3 = \{(a,b,c)\|a<0, b<-1, c<0\}$	Point x^* represents an unstable fixed point, all orbits except that started directly at x^* diverge towards ∞
$\Pi_4 = \{(a,b,c)\|a<0, b>1, c>0\}$	Same as in area Π_3
$\Pi_5 = \{(a,b,c)\|a<0, \|b\|<1, c>0\}$	All orbits diverge towards ∞
$\Pi_6 = \{(a,b,c)\|a<0, b<-1, c>0\}$	Same as in area Π_5
$\Pi_7 = \{(a,b,c)\|a>0, b>1, c<0\}$	All orbits diverge towards $-\infty$
$\Pi_8 = \{(a,b,c)\|a>0, \|b\|<1, c<0\}$	All orbits converge towards the stable fixed point x^*
$\Pi_9 = \{(a,b,c)\|a>0, b<-1, c<0\}$	There is an unstable fixed point x^*, unstable periodic orbits and chaotic attractors
$\Pi_{10} = \{(a,b,c)\|a>0, b>1, c>0\}$	Same as in area Π_9
$\Pi_{11} = \{(a,b,c)\|a>0, \|b\|<1, c>0\}$	There exist several stable periodic orbits
$\Pi_{12} = \{(a,b,c)\|a>0, b<-1, c>0\}$	There are unstable periodic orbits and a chaotic attractor

which maps the real axis $\mathbb{R}$ onto itself. As one can see, the parameter space of system (1) is three-dimensional. One aim of this paper is to describe the structure of this 3D space. Hereby we are mostly interested in periodic orbits of system (1). In order to investigate these orbits, we will use one of the standard symbolic codings for 1D maps (see, for instance, [79]). Hence, a point $x < 0$ is represented by symbol $\mathcal{L}$ and a point $x \geqslant 0$ by symbol $\mathcal{R}$. For a periodic orbit only the sequence corresponding to one period is written. As usual, the resulting symbolic sequences are shift-invariant; therefore, we use sequences starting with the symbol $\mathcal{L}$. Additionally, the limit cycle corresponding to symbolic sequence σ will be denoted as O_σ. The length of the symbolic sequence σ is denoted by $|\sigma|$ and represents the period of the limit cycle O_σ. As $\mathcal{P}_\sigma$ we denote the area in the parameter space, where system (1) possesses the limit cycle O_σ. Note that two areas $\mathcal{P}_\sigma$ and $\mathcal{P}_\varrho$ may overlap. In this case the corresponding limit cycles O_σ and O_ϱ coexist in the overlapping area $\mathcal{P}_\sigma \cap \mathcal{P}_\varrho$. A sequence σ is called admissible for system (1), iff there exists a parameter setting where system (1) possesses the limit cycle O_σ, or, in other words, iff $\mathcal{P}_\sigma \neq \emptyset$.

3. Characteristic areas in the parameter space

Due to the simplicity of the investigated system function, a lot of results concerning its behaviour can be obtained analytically.

Except for the degenerate case $a = 0$, where each point $x > 0$ represents a fixed point, one can see that system (1) can possess maximal one fixed point, which is given by

$$x^* = \frac{c}{1-b} \tag{2}$$

and exists iff the left partial function $f_l(x)$ crosses the bisecting line $f(x) = x$ on its domain $x < 0$. Hence, we state that the point x^* is a fixed point of system (1) iff $x^* < 0$. Obviously, x^* is stable iff $|b| < 1$. It can also be easily shown that stable periodic orbits are possible iff $a > 0$ and $|b| < 1$. Table 1 shows the 12 characteristic areas in the 3D parameter space, which lead to different asymptotic behaviour (see also figure 1).

As one can see, the most interesting areas in the 3D parameter space are Π_9, Π_{10}, Π_{11} and Π_{12}. A significant difference between these areas is that the asymptotic dynamics in

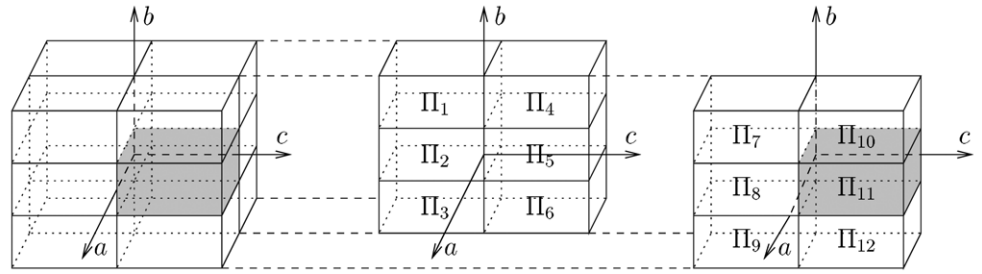

(a) 12 areas in the 3D parameter space

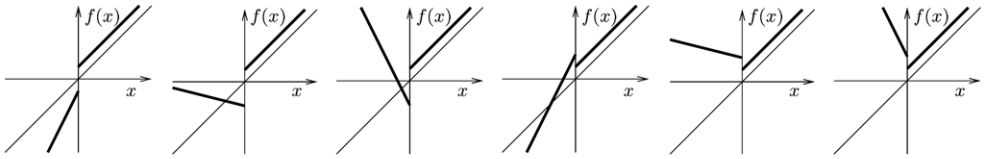

(b) Π_1: $a < 0$, $b > 1$, $c < 0$
(c) Π_2: $a < 0$, $|b| < 1$, $c < 0$
(d) Π_3: $a < 0$, $b < -1$, $c < 0$
(e) Π_4: $a < 0$, $b > 1$, $c > 0$
(f) Π_5: $a < 0$, $|b| < 1$, $c > 0$
(g) Π_6: $a < 0$, $b < -1$, $c > 0$

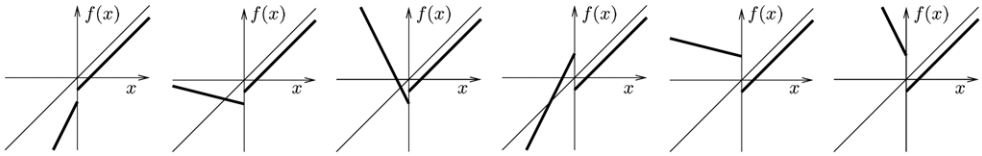

(h) Π_7: $a > 0$, $b > 1$, $c < 0$
(i) Π_8: $a > 0$, $|b| < 1$, $c < 0$
(j) Π_9: $a > 0$, $b < -1$, $c < 0$
(k) Π_{10}: $a > 0$, $b > 1$, $c > 0$
(l) Π_{11}: $a > 0$, $|b| < 1$, $c > 0$
(m) Π_{12}: $a > 0$, $b < -1$, $c > 0$

Figure 1. (*a*) Characteristic areas in the parameter space $[a \times b \times c]$ leading to different asymptotic dynamics. (*b*)—(*m*) Typical shapes of the system function f (equation (1)) in these areas.

the area Π_{11} is periodic, whereas in the areas Π_9, Π_{10} and Π_{12} only chaotic attractors are possible. Some examples of the asymptotic behaviour in these areas are presented in figure 2. For instance, the left part of figure 2(*a*) shows some dynamics in areas Π_9 and Π_{12}. Here we observe a chaotic two-band attractor with some windows, where multi-band chaotic attractors exist. In the right part of figure 2(*a*), which belongs to the area Π_{12}, we observe an impressive grid-like structure, formed by a regular sequence of bifurcations (chaos–chaos transitions), where the number of bands is increased by one at each transition.

The transition from a six-periodic solution to chaos, shown in the left part of figure 2(*b*), is similar to the transition from the fixed point to chaos in the case of the tent map. Varying parameter c from the area Π_{11} to the area Π_{12} at fixed values of a and b, one observes these transitions in system (1) for periodic solutions with arbitrary periods. In the right part of figure 2(*b*) one observes chaotic one-band attractors with regular peaks of the invariant

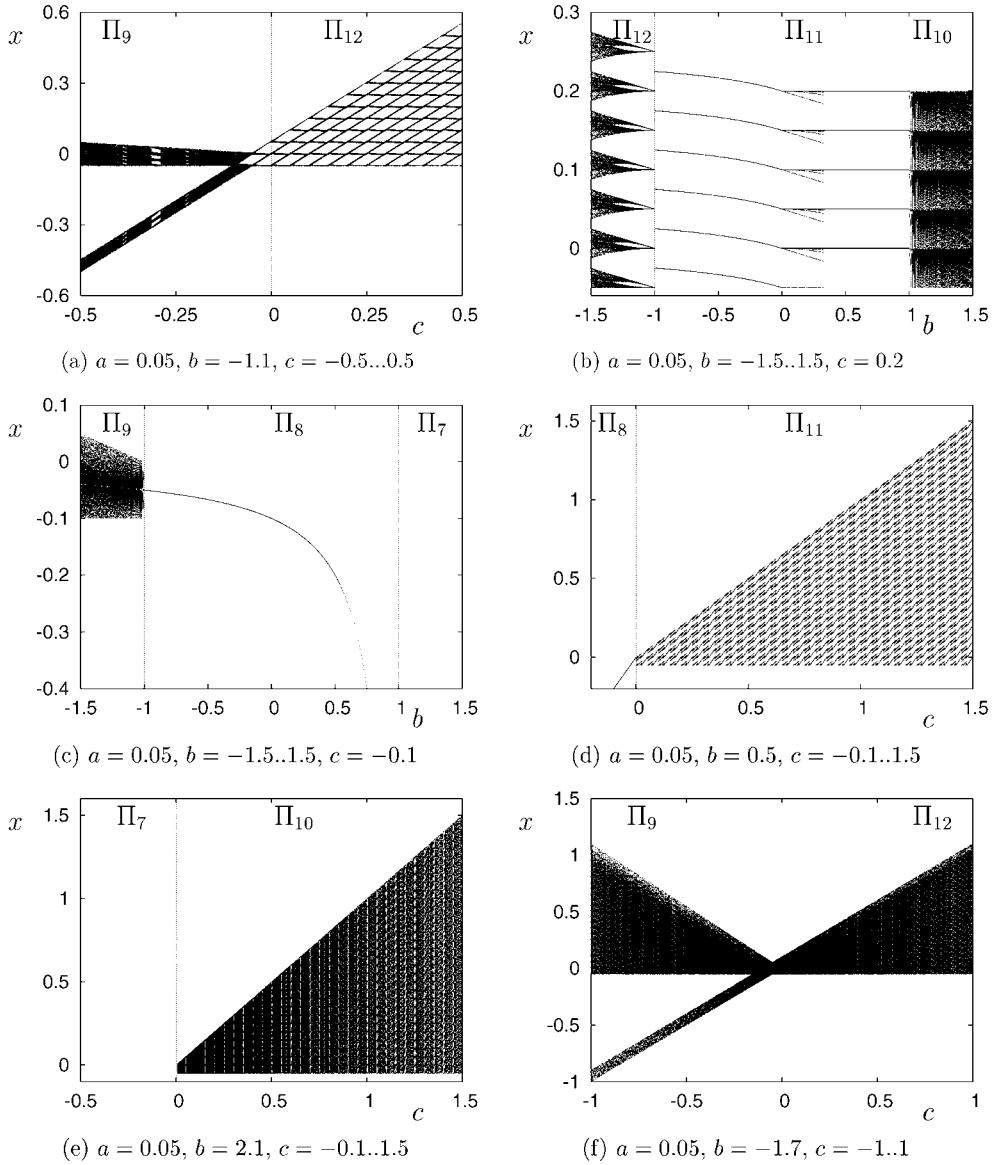

(a) $a = 0.05$, $b = -1.1$, $c = -0.5...0.5$

(b) $a = 0.05$, $b = -1.5..1.5$, $c = 0.2$

(c) $a = 0.05$, $b = -1.5..1.5$, $c = -0.1$

(d) $a = 0.05$, $b = 0.5$, $c = -0.1..1.5$

(e) $a = 0.05$, $b = 2.1$, $c = -0.1..1.5$

(f) $a = 0.05$, $b = -1.7$, $c = -1..1$

Figure 2. Examples for bifurcation scenarios observed in system (1) by variation of only one parameter. Vertical lines mark the borders between areas Π_i, shown in figure 1.

measure. In the presented example these peaks are located at the points $x_k = a \cdot k$ with $k = 0, 1, 2, 3, 4$.

Figure 2(*c*) shows a chaotic one-band attractor in the left part and the fixed point x^* in the middle part. The right part of this figure belongs to the area Π_7, where the orbits diverge towards $-\infty$. Note that the boundaries of the chaotic attractor can be easily calculated and are given by $x_{\min} = c$ and $x_{\max} = f_l(c) = c(b + 1)$. In the special case $b = -1$ (at the boundary between the areas Π_8 and Π_9) system (1) possesses an infinite number of coexisting two-periodic solutions, as is usual for conservative dynamical systems. All these coexisting

limit cycles are located in the interval $[x_{\min}, x_{\max}] = [c, 0]$ In figure 2(*d*) a complex structure of periodic attractors of system (1) is shown. The bifurcation diagram shown in figure 2(*e*) has a shape similar to the previous one but shows only one-band chaotic attractors. Figure 2(*f*) presents one-band attractors in the right part and two-band attractors in the left part.

Obviously, system (1) shows a broad spectrum of different dynamic behaviour and bifurcation scenarios. However, in this work we will concentrate on stable periodic orbits occurring in this system and leave the chaotic attractors for future investigations. Therefore, in the following the area Π_{11} will be considered.

4. Periodic orbits and re-injection mechanism

Next we recall that the mechanism causing the periodic orbits in system (1) to occur is the re-injection mechanism described in [80] (see also [81]). Function $f_r(x)$ forms some kind of channel with the bisecting line $f(x) = x$. Then an orbit performs a number of iteration steps within this channel, leaves it and is afterwards re-injected again into the channel by function $f_l(x)$. For an arbitrary $n > 1$ the resulting limit cycle corresponds to the symbolic sequence $\mathcal{LR}^{n-1}$. One can easily calculate that this limit cycle is given by $O_{\mathcal{LR}^{n-1}} = \{x_i | i = 0, \ldots, n-1\}$ with

$$x_i = \begin{cases} -\dfrac{(n-1)a - c}{1-b} & \text{if } i = 0, \\ bx_0 + c - (i-1)a & \text{if } i = 1, \ldots, n-1 \end{cases} \tag{3}$$

and this existence area in the parameter space is

$$\mathcal{P}_{\mathcal{LR}^{n-1}} = \left\{(a, b, c) : |a^{\min}_{\mathcal{LR}^{n-1}} < a < a^{\max}_{\mathcal{LR}^{n-1}},\ |b| < 1, c > 0\right\}, \tag{4}$$

$$\text{with } a^{\min}_{\mathcal{LR}^{n-1}} = \frac{c}{n-1} \qquad \text{and} \qquad a^{\max}_{\mathcal{LR}^{n-1}} = \frac{c}{n-2+b}. \tag{5}$$

It can also be shown that the limit cycle $O_{\mathcal{LR}^{n-1}}$ is stable in the complete area $\mathcal{P}_{\mathcal{LR}^{n-1}}$ and its Lyapunov exponent is given by

$$\lambda(O_{\mathcal{LR}^{n-1}}) = \frac{1}{n} \ln |b| < 0. \tag{6}$$

A brief sketch of the proof of equations (3)–(6) is presented in the appendix. Note that these equations lead to the following two important results:

(i) For all $n > 1$ the sequence $\mathcal{LR}^{n-1}$ is admissible:

$$\forall n > 1 : \mathcal{P}_{\mathcal{LR}^{n-1}} \neq \emptyset. \tag{7}$$

(ii) For all $n > 1$ the area $\mathcal{P}_{\mathcal{LR}^{n-1}}$ starts at the origin of the plane $[a \times c]$:

$$\forall n > 1 : \lim_{c \to 0} a^{\min}_{\mathcal{LR}^{n-1}} = \lim_{c \to 0} a^{\max}_{\mathcal{LR}^{n-1}} = 0. \tag{8}$$

The next task, which we have to consider in order to investigate the structure of the 3D parameter space $[a \times b \times c]$, is to describe the relative positions of areas $\mathcal{P}_{\mathcal{LR}^{n-1}}$ and $\mathcal{P}_{\mathcal{LR}^{m-1}}$ with respect to each other. This will be done in the next two sections.

Of course, the limit cycles $O_{\mathcal{LR}^{n-1}}$ are not the only possible limit cycles. In general an orbit may perform an arbitrary number of circulations (channel passes) before it is mapped to its starting point again. We denote the number J for these circulations as the re-injection number of the corresponding limit cycle. Consequently, the limit cycle $O_{\mathcal{LR}^{n-1}}$ has the re-injection number $J = 1$. Considering orbits with $J > 1$, we state, for instance, that the limit cycle $O_{\mathcal{LR}^{n-1}\mathcal{LR}^{n}}$ with period $2n + 1$ (for an arbitrary $n > 1$) has the re-injection number $J = 2$. The limit cycle $O_{\mathcal{LR}^{n-1}(\mathcal{LR}^{n})^2}$ with period $3n + 2$ has the re-injection number $J = 3$, etc.

Using the same technique as above we can calculate the limit cycles and their existing areas in the parameter space for $J > 1$. For instance, we obtain for the limit cycles $O_{\mathcal{L}\mathcal{R}^{n-1}\mathcal{L}\mathcal{R}^n} = \{x_i | i = 0, \ldots, 2n\}$ (period $2n + 1$, re-injection number $J = 2$):

$$x_i = \begin{cases} -\dfrac{(n-1)ab + 2na - (b+1)c}{1-b^2} & \text{if } i = 0, \\ bx_0 + c - (i-1)a & \text{if } i = 1, \ldots, n, \\ bx_n + c - (i-1)a & \text{if } i = n+1, \ldots, 2n \end{cases} \tag{9}$$

and

$$\mathcal{P}_{\mathcal{L}\mathcal{R}^{n-1}\mathcal{L}\mathcal{R}^n} = \left\{(a,b,c) | a^{\min}_{\mathcal{L}\mathcal{R}^{n-1}\mathcal{L}\mathcal{R}^n} < a < a^{\max}_{\mathcal{L}\mathcal{R}^{n-1}\mathcal{L}\mathcal{R}^n}, 0 < b < 1, c > 0\right\}, \tag{10}$$

$$\text{with } a^{\min}_{\mathcal{L}\mathcal{R}^{n-1}\mathcal{L}\mathcal{R}^n} = \frac{(b+1)c}{2n + (n-1)b} \qquad \text{and} \qquad a^{\max}_{\mathcal{L}\mathcal{R}^{n-1}\mathcal{L}\mathcal{R}^n} = \frac{(b+1)c}{(2+b)n + b^2 - b - 1}. \tag{11}$$

As in the case before, the limit cycles $O_{\mathcal{L}\mathcal{R}^{n-1}\mathcal{L}\mathcal{R}^n}$ are stable in the complete area $\mathcal{P}_{\mathcal{L}\mathcal{R}^{n-1}\mathcal{L}\mathcal{R}^n}$, because their Lyapunov exponent is negative:

$$\lambda(O_{\mathcal{L}\mathcal{R}^{n-1}\mathcal{L}\mathcal{R}^n}) = \frac{2}{2n+1} \ln|b| < 0. \tag{12}$$

The following results are important:

(i) For all $n > 1$ the sequence $\mathcal{L}\mathcal{R}^{n-1}\mathcal{L}\mathcal{R}^n$ is admissible, iff $b > 0$:

$$b > 0 \Rightarrow \forall n > 1 : \mathcal{P}_{\mathcal{L}\mathcal{R}^{n-1}\mathcal{L}\mathcal{R}^n} \neq \emptyset. \tag{13}$$

(ii) For all $n > 1$ the area $\mathcal{P}_{\mathcal{L}\mathcal{R}^{n-1}\mathcal{L}\mathcal{R}^n}$ starts at the origin of the plane $[a \times c]$:

$$\forall n > 1 : \lim_{c \to 0} a^{\min}_{\mathcal{L}\mathcal{R}^{n-1}\mathcal{L}\mathcal{R}^n} = \lim_{c \to 0} a^{\max}_{\mathcal{L}\mathcal{R}^{n-1}\mathcal{L}\mathcal{R}^n} = 0.$$

(iii) The area $\mathcal{P}_{\mathcal{L}\mathcal{R}^{n-1}\mathcal{L}\mathcal{R}^n}$ is located between the areas $\mathcal{P}_{\mathcal{L}\mathcal{R}^{n-1}}$ and $\mathcal{P}_{\mathcal{L}\mathcal{R}^n}$:

$$\forall n > 1 : a^{\max}_{\mathcal{L}\mathcal{R}^n} < a^{\min}_{\mathcal{L}\mathcal{R}^{n-1}\mathcal{L}\mathcal{R}^n} < a^{\max}_{\mathcal{L}\mathcal{R}^{n-1}\mathcal{L}\mathcal{R}^n} < a^{\min}_{\mathcal{L}\mathcal{R}^{n-1}}.$$

Similar results can be obtained for $J > 2$ as well. Note that the the calculation becomes more complicated for increasing re-injection numbers but remains possible, because all involved functions are linear with respect to x. In general, if $N_{\mathcal{L}}(\sigma)$ and $N_{\mathcal{R}}(\sigma)$ are the numbers of symbols $\mathcal{L}$ and $\mathcal{R}$ in the symbolic sequence σ, then the Lyapunov exponent of the limit cycle O_σ is given by

$$\lambda(O_\sigma) = \frac{N_{\mathcal{L}}(\sigma)}{N_{\mathcal{L}}(\sigma) + N_{\mathcal{R}}(\sigma)} \ln|b| < 0 \tag{14}$$

(see figure 3). This result can be obtained in analogy to equation (6). As a consequence we state that in the case $b = 0$ the limit cycles of system (1) are super-stable for all values of the parameters $a > 0$ and $c > 0$.

5. Structure of 2D parameter subspaces

After the areas in the parameter space leading to specific periodic dynamics are determined analytically, we can explain the structure of the complete 3D area Π_{11}. For simplicity of explanation, we consider the three characteristic cases $b = 0$, $b < 0$ and $b > 0$ separately and describe firstly the bifurcation structures in the plane $[a \times c]$ for these three cases.

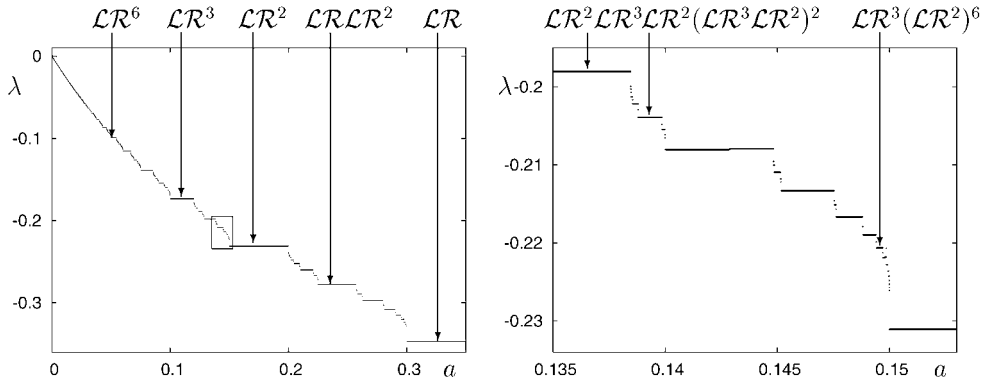

(a) (b)

σ	$N_{\mathcal{L}}(\sigma)$	$N_{\mathcal{R}}(\sigma)$	λ
$\mathcal{LR}^6$	1	6	≈ -0.099021
$\mathcal{LR}^3$	1	3	≈ -0.173289
$\mathcal{LR}^2$	1	2	≈ -0.231049
$\mathcal{LRLR}^2$	2	3	≈ -0.277259
$\mathcal{LR}$	1	1	≈ -0.346573
$\mathcal{LR}^2\mathcal{LR}^3$	2	5	≈ -0.198042
$\mathcal{LR}^2(\mathcal{LR}^3\mathcal{LR}^2)^2$	5	12	≈ -0.203867
$\mathcal{LR}^3(\mathcal{LR}^2)^6$	7	15	≈ -0.220547

Figure 3. Under variation of the parameter a the Lyapunov exponent λ shows the typical devil's staircase structure. Symbolic sequences of attractors for some values are presented, whereby the analytical calculated value of λ (see equation (14)) is shown in the table. The rectangle marked in (a) is shown enlarged in (b). Parameter values $b = 0.5$, $c = 0.3$.

5.1. Case $b = 0$

From equation (5), we yield in the case $b = 0$

$$\forall n > 1 : a^{\min}_{\mathcal{LR}^n} < a^{\max}_{\mathcal{LR}^n} = a^{\min}_{\mathcal{LR}^{n-1}} < a^{\max}_{\mathcal{LR}^{n-1}}. \tag{15}$$

Schematically this result can be represented as follows:

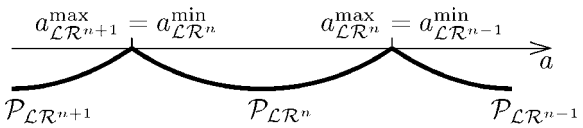

Therefore, the investigated area in the 2D parameter space $[a \times c]$ is covered by regions $\mathcal{P}_{\mathcal{LR}^{n-1}}$, which are disjunct in the case $b = 0$. Equation (8) implies that all these regions start at the origin of the $[a \times c]$ plane, so that in any arbitrary small open neighbourhood of the origin an infinite number of different periodic dynamics exists.

Figure 4 demonstrates the structure of the area Π_{11} in the case $b = 0$. In figure 4(a) some of the areas $\mathcal{P}_{\mathcal{LR}^{n-1}}$ are marked. One can clearly see that all these areas have a triangular shape and start at the origin. Additionally, figures 4(b) and (c) show the bifurcation and period

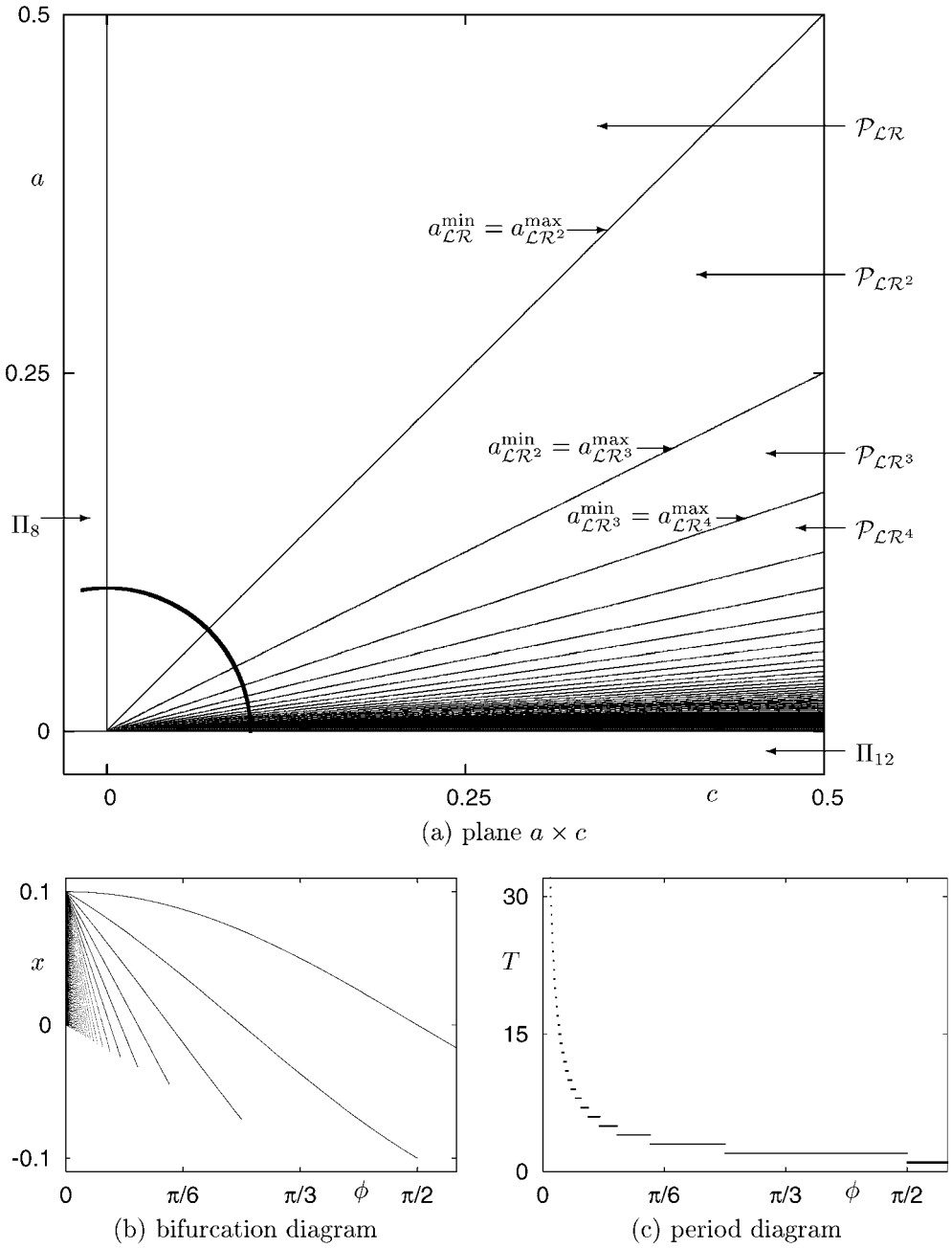

Figure 4. (*a*) Structure of the area Π_{11} in the 2D parameter space $[a \times c]$ (unfolding of the two-parametric bifurcation at the origin) in the case $b = 0$. Marked are some of the bifurcation curves $a^{\min}_{\mathcal{LR}^n}$ and $a^{\max}_{\mathcal{LR}^n}$ (see equation (5)) and the corresponding regions $\mathcal{P}_{\mathcal{LR}^n}$. (*b*) and (*c*) Bifurcation and period diagram of the bifurcation scenario along the curve around the origin marked in (*a*).

diagrams along the curve marked in figure 4(*a*) (a part of the circle given by $a = R\sin(\phi)$, $c = R\cos(\phi)$ with radius $R = 0.1$ and $\phi = 0\ldots 5\pi/9$). The bifurcation scenario along this curve is caused by a sequence of border collision bifurcations, whereby the periods of the limit cycles in this sequence are given by $p_n = p_0 + n\Delta p$ with the starting period p_0 and the increment value Δp (see fig 4(*c*)). In the case presented the starting period and the increment value are both equal to one. This scenario is denoted as the period-increment scenario and represents a phenomenon which is typical for dynamical systems with a piecewise-smooth system function.

Note additionally, that in the left part of figure 4(*a*) the area Π_8 is shown, where the asymptotic dynamic of system (1) is given by the stable fixed point x^* (see section 3). In figure 4(*b*) we observe that at the border collision bifurcation line $a^{\min}_{\mathcal{LR}}$ (vertical axis $c = 0$, $a > 0$) this fixed point becomes a part of the limit cycle $O_{\mathcal{LR}}$. This phenomenon is typical for dynamical systems with a piecewise-smooth system function (see, for instance, [82]) and represents a remarkable difference between these systems and classical smooth systems. In smooth dynamical systems a fixed point may change its stability or disappear at the bifurcation point but is not incorporated into an attractor after the bifurcation.

5.2. *Case* $-1 < b < 0$

In this case we obtain from equation (5) that for any $c > 0$ the following holds:

$$\forall n > 1 : a^{\min}_{\mathcal{LR}^n} < a^{\max}_{\mathcal{LR}^{n+1}} < a^{\min}_{\mathcal{LR}^{n-1}} < a^{\max}_{\mathcal{LR}^n}. \tag{16}$$

The following scheme shows the relative locations of the parameter intervals, where the limit cycles $O_{\mathcal{LR}^{n+1}}$, $O_{\mathcal{LR}^n}$, $O_{\mathcal{LR}^{n-1}}$, etc exists.

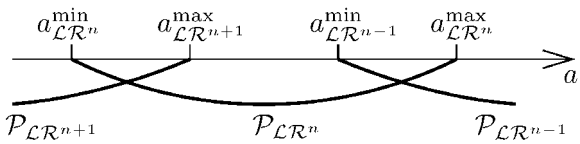

As a consequence, for all $n > 1$ the limit cycles $O_{\mathcal{LR}^{n-1}}$ and $O_{\mathcal{LR}^n}$ coexist in the interval $a^{\min}_{\mathcal{LR}^{n-1}}, \ldots, a^{\max}_{\mathcal{LR}^n}$. Therefore, the investigated area in the parameter space is covered again by regions $\mathcal{P}_{\mathcal{LR}^{n-1}}$, which are however not disjunct in the case $b < 0$. All these regions start at the origin of the $[a \times c]$ plane, so that in any arbitrary small open neighbourhood of the origin an infinite number of different periodic dynamics exists.

Figure 5 demonstrates the structure of the area Π_{11} described above. In figure 5(*a*) some of the areas $\mathcal{P}_{\mathcal{LR}^{n-1}}$ and the overlapping areas $\mathcal{P}_{\mathcal{LR}^{n-1}} \cap \mathcal{P}_{\mathcal{LR}^n}$ are shown. One can clearly see that all these areas have a triangular shape and start at the origin. Additionally, figures 5(*b*) and (*c*) show the bifurcation and period diagrams along the curve marked in figure 5(*a*). This bifurcation scenario represents again the period increment phenomenon; however, in this case the coexistence of attractors can be observed. Especially, there exists a parameter interval where the fixed point x^* coexists with the two-periodic limit cycle $O_{\mathcal{LR}}$.

5.3. *Case* $0 < b < 1$

In this case we yield from equation (5) for any $c > 0$:

$$\forall n > 1 : a^{\min}_{\mathcal{LR}^{n+1}} < a^{\max}_{\mathcal{LR}^{n+1}} < a^{\min}_{\mathcal{LR}^n} < a^{\max}_{\mathcal{LR}^n}. \tag{17}$$

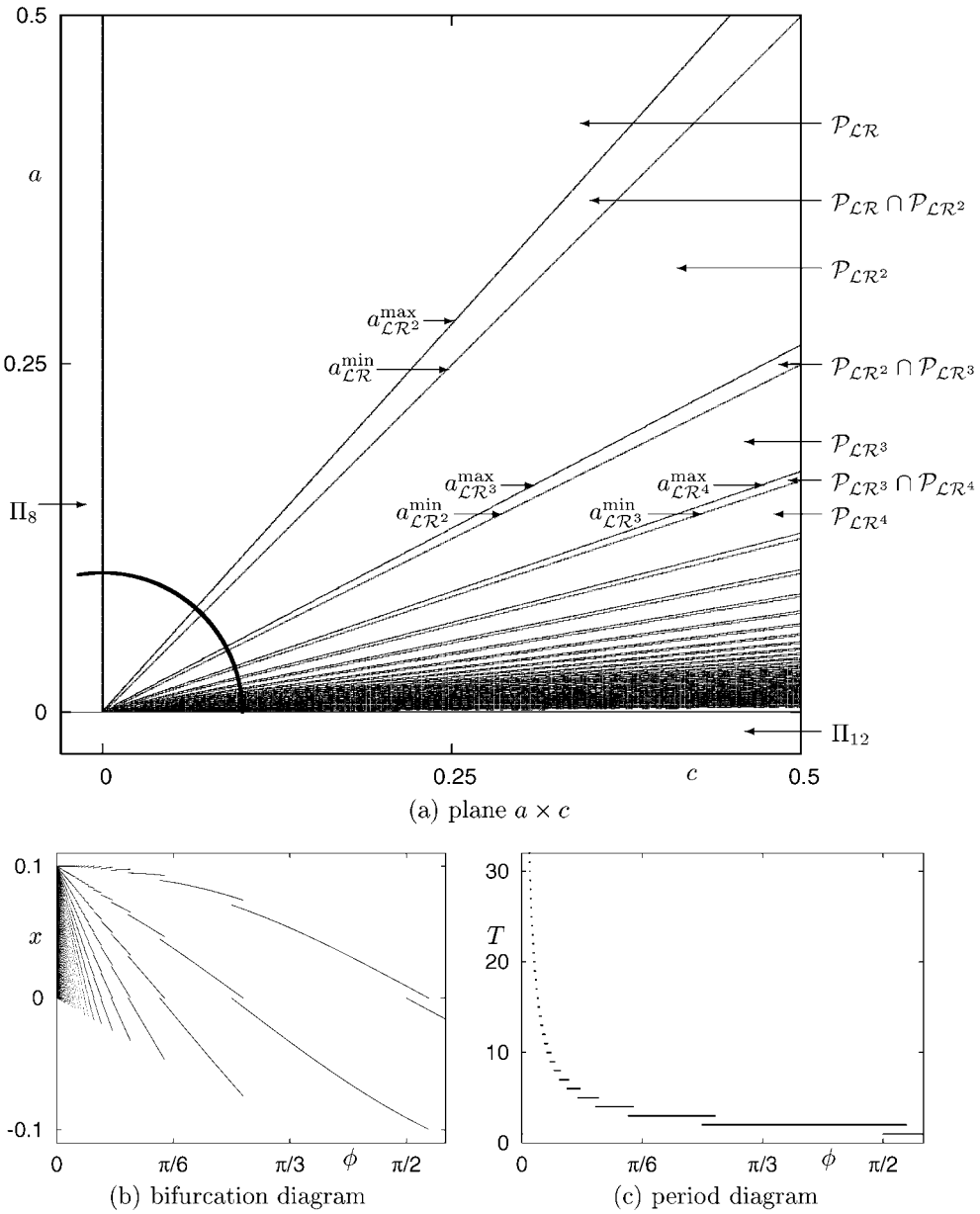

Figure 5. (*a*) Structure of the area Π_{11} in the 2D parameter space $[a \times c]$ (unfolding of the two-parametric bifurcation at the origin) in the case $b < 0$. Marked are some of the bifurcation curves $a^{\min}_{\mathcal{LR}^n}$ and $a^{\max}_{\mathcal{LR}^n}$ (see equation (5)) and the corresponding regions $\mathcal{P}_{\mathcal{LR}^n}$. (*b*) and (*c*) Bifurcation and period diagram of the bifurcation scenario along the curve around the origin marked in (*a*).

This result corresponds to the following scheme:

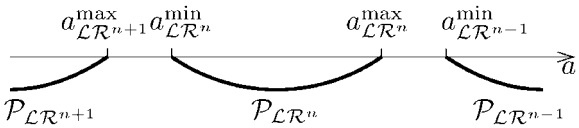

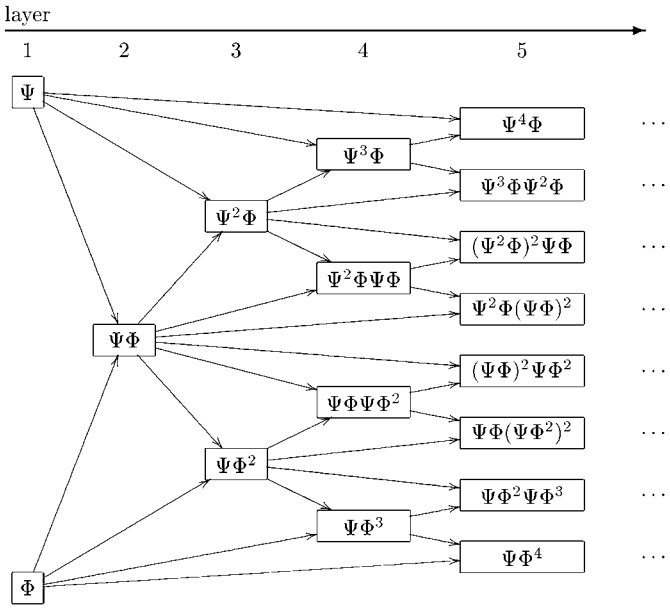

Figure 6. First layers of the infinite adding scheme generating admissible symbolic sequences. Letters Ψ and Φ denote sequences $\mathcal{L}^n\mathcal{R}$ and $\mathcal{L}^{n-1}\mathcal{R}$. See section 5.3 for a detailed description.

In this case, the investigated area in the parameter space is not covered by regions $\mathcal{P}_{\mathcal{L}\mathcal{R}^{n-1}}$. We state in this case that between each two subsequent areas $\mathcal{P}_{\mathcal{L}\mathcal{R}^{n-1}}$ and $\mathcal{P}_{\mathcal{L}\mathcal{R}^n}$ there is a 'free space' (see figure 7). From equation (4) it follows that the area $\mathcal{P}_{\mathcal{L}\mathcal{R}^{n-1}\mathcal{L}\mathcal{R}^n}$ is located here. However, between the areas $\mathcal{P}_{\mathcal{L}\mathcal{R}^{n-1}}$ and $\mathcal{P}_{\mathcal{L}\mathcal{R}^{n-1}\mathcal{L}\mathcal{R}^n}$, as well as between the areas $\mathcal{P}_{\mathcal{L}\mathcal{R}^n}$ and $\mathcal{P}_{\mathcal{L}\mathcal{R}^{n-1}\mathcal{L}\mathcal{R}^n}$, there is still 'free space'. Therefore, the question arises, which symbolic sequences σ are admissible for system (1) and how the corresponding areas $\mathcal{P}_\sigma$ are located relative to each other. A detailed discussion concerning this topic is beyond the scope of this paper (see, for instance, [82] for a more detailed description). We state that a sequence σ is admissible for system (1) if it can be derived from the sequences $\mathcal{P}_{\mathcal{L}^{n-1}\mathcal{R}}$ and $\mathcal{P}_{\mathcal{L}^n\mathcal{R}}$ for some n using the *infinite adding scheme*. This scheme is also related to the well-known Farey-trees [83]. The first layers of this scheme are shown in figure 6. The scheme can be continued layer-wise *ad infinitum* according to the following simple rule: a symbolic sequence in the nth layer is constructed via concatenation of a sequence from the $(n-1)$th layer with the corresponding direct successor of this sequence.

From the construction rule the following property of the infinite adding scheme can be obtained: if a sequence $\sigma = \varrho\varpi$ is constructed within this scheme and has direct successors ϱ and ϖ that correspond to limit cycles with periods $p_1 = |\varrho|$ and $p_2 = |\varpi|$ and re-injection numbers J_1 and J_2, then the sequence σ corresponds to a limit cycle with period $p_1 + p_2$ and re-injection number $J_1 + J_2$. This is important, because there exists a bijective mapping between the parameter space of system (1) and the space of admissible symbolic sequences generated within the infinite adding scheme described above. Namely, if σ is an admissible symbolic sequence with direct successors ϱ and ϖ, then the area $\mathcal{P}_\sigma$ lies between the areas $\mathcal{P}_\varrho$ and $\mathcal{P}_\varpi$ in the parameter space $[\alpha \times \beta]$.

Let us consider additionally the bifurcation line $a_{\max}^{\mathcal{L}\mathcal{R}}$ bounding the area $\mathcal{P}_{\mathcal{L}\mathcal{R}}$ from the left. In the case $b = 0$ this bifurcation line is identical to vertical axis $c = 0$, which confines the investigated area Π_{11}. For $b > 0$ the line $a_{\max}^{\mathcal{L}\mathcal{R}}$ has a finite slope, so that a region of the

parameter space between this line and the vertical axis $c = 0$ emerges. In this region we observe the areas $\mathcal{P}_{\mathcal{L}^{n-1}\mathcal{R}}$ for all $n > 2$ as well as the areas $\mathcal{P}_\sigma$, whereby the sequence σ can be derived from a pair $\mathcal{L}^{n-1}\mathcal{R}$, $\mathcal{L}^n\mathcal{R}$ for some n. The structure of this region is analogue to the one of the area below the bifurcation line $a_{\min}^{\mathcal{LR}}$. Hereby analogue means that the symbols $\mathcal{L}$ and $\mathcal{R}$ in the admissible sequences σ are exchanged.

6. Structure of the complete 3D parameter space

Our next goal is to combine the results obtained for the 2D parameter subspaces $[a \times c]$ in the cases $b < 0$, $b = 0$ and $b > 0$ and to describe the structure of the area Π_{11} in the complete 3D parameter space $[a \times b \times c]$. Let us consider the relative positions of the two areas $\mathcal{P}_{\mathcal{LR}^{n-1}}$ and $\mathcal{P}_{\mathcal{LR}^n}$ in the 3D parameter space (see figure 8). These areas are schematically represented by the polyhedrons $A_1A_3A_0C_0C_1C_2$ and $A_2A_4A_0C_0C_3C_4$, which are bounded by the corresponding bifurcation planes. Note that the three horizontal planes shown in the figure represent the three cases $b < 0$, $b = 0$ and $b > 0$ mentioned above and are related to the numeric results presented in figures 4, 5 and 7.

As one can see, below the plane $b = 0$ the polyhedrons $A_1A_3A_0C_0C_1C_2$ and $A_2A_4A_0C_0C_3C_4$ overlap, and hence in the area $A_2A_3A_0B_0B_2$ the limit cycles $O_{\mathcal{LR}^{n-1}}$ and $O_{\mathcal{LR}^n}$ coexist. By movement of the parameter b from negative to positive values (upwards in figure 8), the areas $\mathcal{P}_{\mathcal{LR}^{n-1}}$ and $\mathcal{P}_{\mathcal{LR}^n}$ shrink and consequently also the overlapping area $\mathcal{P}_{\mathcal{LR}^{n-1}} \cap \mathcal{P}_{\mathcal{LR}^n}$. It is clearly shown that plane $b = 0$ bounds the overlapping area from above, so that there are no coexisting limit cycles for all parameter values $b \geqslant 0$. For increasing positive values of parameter b, the areas $\mathcal{P}_{\mathcal{LR}^{n-1}}$ and $\mathcal{P}_{\mathcal{LR}^n}$ continue to shrink, and the area in between (represented in the figure by the polyhedron $B_2B_0C_0C_2C_3$) increases. As we already know, in this area the limit cycles with re-injection number $J > 1$ emerge.

The results of the numerical validation of the described phenomenon are presented in figure 9. Here parameters a and c are varied along the curve marked in figures 4(a), 5(a) and 7(a), given by a part of a circle ($a = R\sin(\phi)$, $c = R\cos(\phi)$ with $R = 0.1$ and $\phi = 0, \ldots, \pi/2$). Simultaneously parameter b is varied as well. Hence, the bifurcation scenarios presented in figures 4(b), 5(b) and 7(b) take place along the horizontal lines marked in figure 9. Due to the fact that the dependence of $a_\sigma^{\min}$ and $a_\sigma^{\max}$ on the parameter c is linear for all admissible sequences σ, the structure presented in figure 9 does not depend on the radius R. Based on equation (4) we obtain the curves $\phi_{\min}^{\mathcal{LR}^{n-1}}$ and $\phi_{\max}^{\mathcal{LR}^{n-1}}$ bounding the regions $\mathcal{P}_{\mathcal{LR}^{n-1}}$ in the cylindrical surface $[\phi \times b]$:

$$\phi_{\min}^{\mathcal{LR}^n} = \arctan\left(\frac{1}{n-1}\right) \qquad \text{and} \qquad \phi_{\max}^{\mathcal{LR}^n} = \arctan\left(\frac{1}{n-2+b}\right). \tag{18}$$

These values are defined analogously to the values $a_{\min}^{\mathcal{LR}^n}$ and $a_{\max}^{\mathcal{LR}^n}$. We state especially that the values $\phi_{\min}^{\mathcal{LR}^n}$ do not depend on b, i.e. they are represented by vertical lines in figure 9. The overlapping area $\mathcal{P}_{\mathcal{LR}^{n-1}} \cap \mathcal{P}_{\mathcal{LR}^n}$ is clearly visible for parameter values $b < 0$ as well as the area leading to limit cycles with $J > 1$ for parameter values $b > 0$. Remarkably, for each n, the point at the horizontal line $b = 0$, where the line $\phi_{\min}^{\mathcal{LR}^{n-1}}$ intersects the curve $\phi_{\max}^{\mathcal{LR}^n}$, represents the same type of singularity in the $[\phi \times b]$ surface as the origin of the plane $[a \times c]$ shown in figures 4(a), 5(a) and 7(a). Namely, in any arbitrary small open neighbourhood of each of these points there is an infinite number of different periodic dynamics, given by limit cycles with $J > 1$. Therefore, these singularities are considered in the next section in more detail.

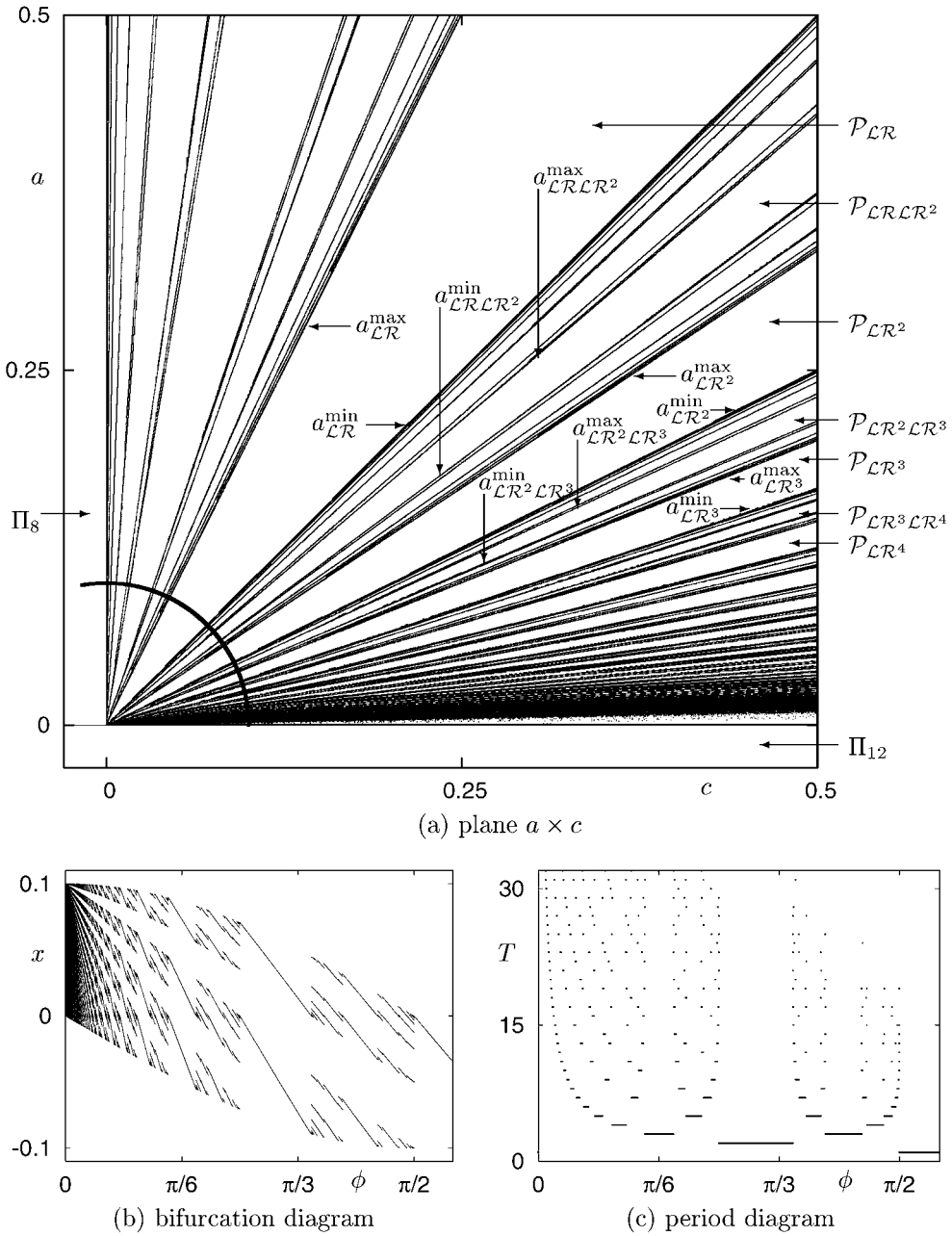

Figure 7. (*a*) Structure of the area Π_{11} in the 2D parameter space $[a \times c]$ (unfolding of the two-parametric bifurcation at the origin) in the case $b > 0$. Marked are some of the bifurcation curves $a^{\min}_{\mathcal{LR}^n}$ and $a^{\max}_{\mathcal{LR}^n}$ (see equation (5)) and the corresponding regions $\mathcal{P}_{\mathcal{LR}^n}$. Additionally some of the bifurcation curves $a^{\min}_{\mathcal{LR}^{n-1}\mathcal{LR}^n}$ and $a^{\max}_{\mathcal{LR}^{n-1}\mathcal{LR}^n}$ (see equation (11)) and the corresponding regions $\mathcal{P}_{\mathcal{LR}^{n-1}\mathcal{LR}^n}$ are marked as well. (*b*) and (*c*) Bifurcation and period diagram of the bifurcation scenario along the curve around the origin marked in (*a*).

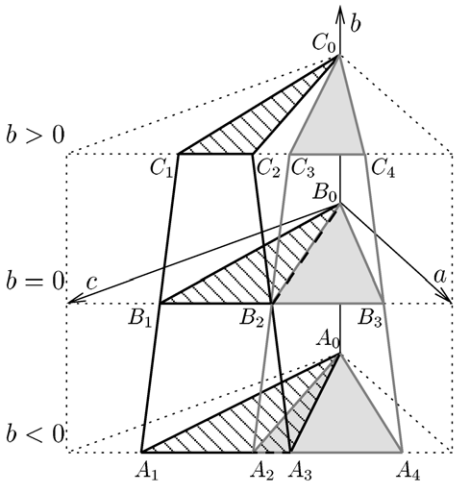

polyhedron	asymptotic dynamics
$A_1A_3A_0C_0C_1C_2$	$O_{\mathcal{LR}^n}$
$A_2A_4A_0C_0C_3C_4$	$O_{\mathcal{LR}^{n-1}}$
$A_2A_3A_0B_0B_2$	$O_{\mathcal{LR}^{n-1}}$ and $O_{\mathcal{LR}^n}$ (coexisting)
$B_2B_0C_0C_2C_3$	O_σ, where σ can be derived from $\mathcal{LR}^{n-1}$ and $\mathcal{LR}^n$ using the infinite adding scheme

plane	bifurcation plane
$A_1A_0C_0C_1$	$a^{\min}_{\mathcal{LR}^n}$
$A_1A_0C_0C_1$	$a^{\max}_{\mathcal{LR}^n}$
$A_1A_0C_0C_1$	$a^{\min}_{\mathcal{LR}^{n-1}}$
$A_1A_0C_0C_1$	$a^{\max}_{\mathcal{LR}^{n-1}}$

Figure 8. Schematic representation of the structure of the 3D parameter space $[a \times b \times c]$ of the piecewise-linear map (1) in the vicinity of the origin: two-parametric bifurcations along the lines A_0C_0, B_0B_1, B_0B_2, B_0B_3 and a three-parametric bifurcation at the point B_0.

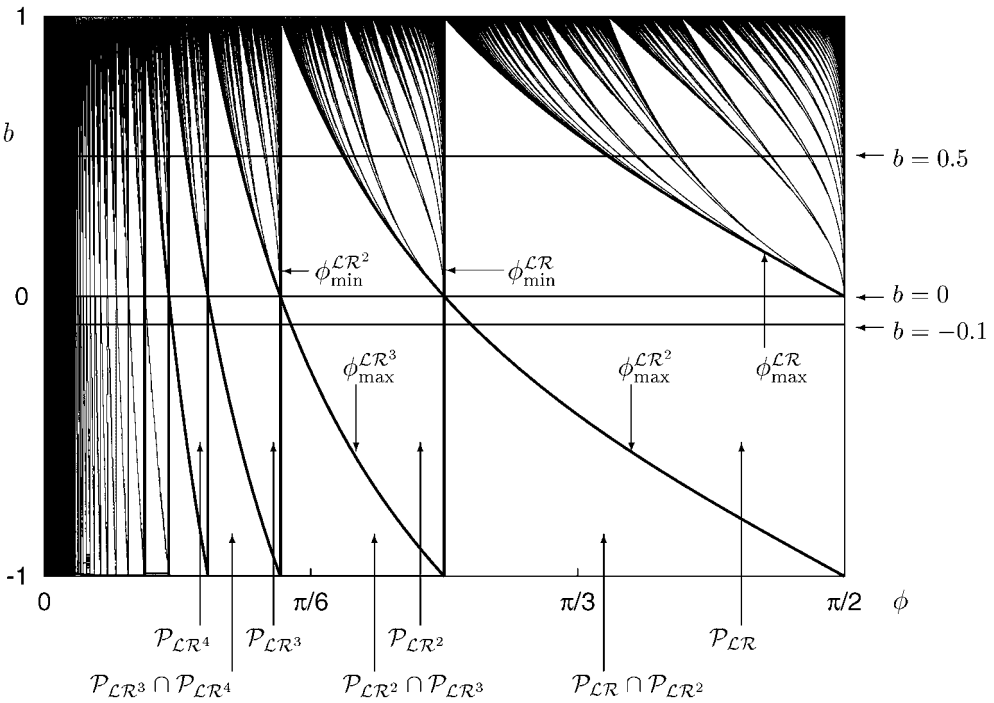

Figure 9. Regions $\mathcal{P}_\sigma$ in the $[\phi \times b]$ surface (cylindrical surface around the b-axis of the 3D parameter space $[a \times b \times c]$). Horizontal lines marked on the right side with the values of b correspond to figures 4, 5 and 7. Marked are some of the bifurcation curves $\phi^{\min}_{\mathcal{LR}^n}$ and $\phi^{\max}_{\mathcal{LR}^n}$ (see equation (18)) and the corresponding regions $\mathcal{P}_{\mathcal{LR}^n}$.

7. Multi-parametric bifurcations

Now the results obtained so far must be interpreted in a more general context. Let us first recall some basic notation. According to the standard definition, one can denote as a bifurcation point a point in the parameter space, where the asymptotic dynamics of a dynamical system undergoes a qualitative change. In other words, in an arbitrary small open vicinity of the bifurcation point there exist exactly two different asymptotic dynamics. Investigating 1D parameter spaces, there is no need to introduce any more complex notation. However, when dealing with 2D parameter spaces, the situation becomes more sophisticated. Bifurcation curves in a 2D parameter space confine areas leading to different asymptotic dynamics, so that any 1D parameter study through a point on such a curve corresponds typically to the standard situation described above. An exception is given by the points where several bifurcation curves intersect. In this case, in an arbitrary small open vicinity of these bifurcation points there may exist more than two different asymptotic dynamics. Performing any 1D parameter study through such a point, one can observe at most two of these dynamics. It should be emphasized that the dynamics, which are observed within a 1D parameter study in this case, are specific for the direction of this study and not only for the bifurcation point itself. For this reason, such a bifurcation can be adequately described only in a 2D parameter space and not in a 1D one. Therefore, it has to be denoted as a two-parametric or co-dimension two bifurcation.

The special case of the two-parametric bifurcation, which we are most interested in, is given by the situation that in any open vicinity of the bifurcation point an infinite number of different asymptotic dynamics exists. In [84] it is suggested to denote these points as *big bang bifurcations*. More precisely, a big bang bifurcation point in a 2D parameter space is defined as a point, where an infinite number of bifurcation curves intersect. This definition seems to be more correct than the one used in [84, 85], because it also includes the case where the number of different dynamics in an arbitrary small vicinity is finite, but the number of bifurcation curves is infinite. In the literature we know so far, this case is not reported, but it can be easily constructed[1]. The used definition of the big bang bifurcation does not specify which kind of asymptotic dynamics is involved. A more precise classification of big bang bifurcations can be obtained according to the one-parametric bifurcation scenario taking place along the border of an infinite small convex open vicinity of the bifurcation point. Until now, we have detected some dynamical systems, which show along this border such bifurcation scenarios as period doubling, period increment and period adding [85] (see also [81]). For instance, the piecewise-quadratic map, introduced in [27, 86] as a special kind of Poincaré return map of the Lorenz system, shows an infinite number of big bang bifurcations with the period adding scenario along the border of the vicinity mentioned above.

Of course, there exist not only two-, but also n-parametric (or co-dimension n) bifurcations. According to [50, 60], the co-dimension of a bifurcation is defined as the difference between the parameter space dimension and the dimension of the bifurcation's domain, i.e. the dimension of the subset of parameters, where the bifurcation occurs. An important question arising in this context is how the co-dimension of a bifurcation can be practically determined. It is beyond the scope of this paper to discuss this topic in full detail; therefore, we restrict ourselves to a brief sketch of the basic ideas. Let us consider a bifurcation point A in the n-dimensional

[1] One can consider the map $x_{n+1} = 2x_n \sin(1/\varphi)$ with the 2D parameter plane $[a \times b] = R^2$ and $\varphi = \arctan(a/b)$. This map has only four different asymptotic dynamics. For $|\sin(1/\varphi)| < 1$ its orbits converge to zero; for $|\sin(1/\varphi)| > 1$ the orbits diverge to infinity. Additionally, in the case $\sin(1/\varphi) = 1$ the map has an infinite number of fixed points and in the case $\sin(1/\varphi) = -1$ an infinite number of two-periodic solutions, depending on the initial value. However, at the origin of the parameter space $[a \times b]$ an infinite number of bifurcation curves intersect.

parameter space $\Theta = [\theta_1 \times \cdots \times \theta_n] \subseteq R^n$. Let further

$$\Theta_i = [\theta_1 \times \cdots \times \theta_{i-1} \times \theta_{i+1} \times \cdots\cdots \times \theta_n] \subseteq R^{n-1}, \qquad i = 1, \cdots, n$$

be $(n-1)$-dimensional subspaces of Θ (i.e. for all i it holds $\Theta = [\Theta_i \times \theta_i]$), with $A \in \Theta_i$ for all i. Then, the point A is a point of an n-parametric bifurcation, if for all i the topological structure of Θ_i and the corresponding asymptotic dynamics are changed at the point A by an infinitesimal variation of the parameter θ_i. A more detailed investigation of this topic is left for future work; however, the description presented above allows us to distinguish between two- and three-parametric bifurcations for the investigated piecewise-linear map.

Let us start with the bifurcation lines in the planes $[a \times c]$ for the case $b \neq 0$. All these lines start at the origin of the corresponding plane $[a \times c]$, and obviously each point of these lines, except the origin, represents a one-parametric bifurcation point. Next we consider the origin of the plane $[a \times c]$ for $b \neq 0$. In figure 8 these points are shown at the line A_0C_0 (we do not consider here point B_0, representing the origin of the complete 3D parameter space, because this point corresponds to $b = 0$). In the case $-1 < b < 0$, at the point $a = 0$, $c = 0$ a period increment big bang bifurcation occurs, whereas in the case $0 < b < 1$ this point represents a period adding big bang bifurcation. Note that these bifurcations are two-parametric, and not three-parametric, because a variation of the third parameter b in the corresponding intervals $-1 < b < 0$ and $0 < b < 1$ does not affect the topological structure of the parameter space $[a \times c]$.

Next let us consider the points at the bifurcation lines in the planes $[a \times c]$ for the case $b = 0$. Considering only this plane, one can assume that the bifurcations occurring at these points are one-parametric. However, considering these points in the 3D parameter space, we observe an infinite number of regions $\mathcal{P}_\sigma$ starting at these points where O_σ represents a limit cycle with the re-injection number $J > 1$. Therefore each of these points is a point of a two-parametric bifurcation. This fact becomes clearly visible in the planes $[a \times b]$ and $[b \times c]$ (also compare figure 9).

Another situation takes place at the origin $a = b = c = 0$. We have already stated that under variation of the parameter b the topological structure of the parameter subspace $[a \times c]$ is changed at this point. For $b < 0$ this structure is dominated by the big bang bifurcation with the period increment scenario around the bifurcation point, as shown in figure 5. In contrast, for $b > 0$ this structure is determined by the big bang bifurcation with the adding increment scenario around the bifurcation point, as shown in figure 7. A qualitative change of the asymptotic dynamics can also be observed under variation of a for the parameter subspace $[b \times c]$ as well as under variation of c for the parameter subspace $[a \times b]$. Namely, varying the parameter a from negative to positive values in the vicinity of the origin, one shifts the system from the areas Π_2 and Π_5 into the areas Π_8 and Π_{11}. As mentioned in section 3, the asymptotic dynamics in these areas is different. A similar result holds for the variation of c from negative to positive values in the vicinity of the origin. Therefore, the bifurcation at the origin is in fact three-parametric. This fact becomes clearly visible in figure 10, which combines the numerical results presented above. Horizontal planes in this figure correspond to figures 4, 5, 7, whereas the cylindrical surface around the b-axis corresponds to figure 9. As one can see, the bifurcation lines presented in figure 4 (i.e. in the middle plane in figure 10) are in fact two-parametric and intersect each other at the origin.

Summarizing the results, we state that a single three-parametric bifurcation at the origin causes an infinite number of bifurcation lines to emerge (see figure 4(*a*)), whereby each point of these lines represents a two-parametric bifurcation as shown in figure 9. Note that figure 9 shows the situation in the $[b \times \phi]$ subspace and hence the bifurcation lines shown in figure 4(*a*) are in this case represented by points on the line $b = 0$ given by the intersection of the curves

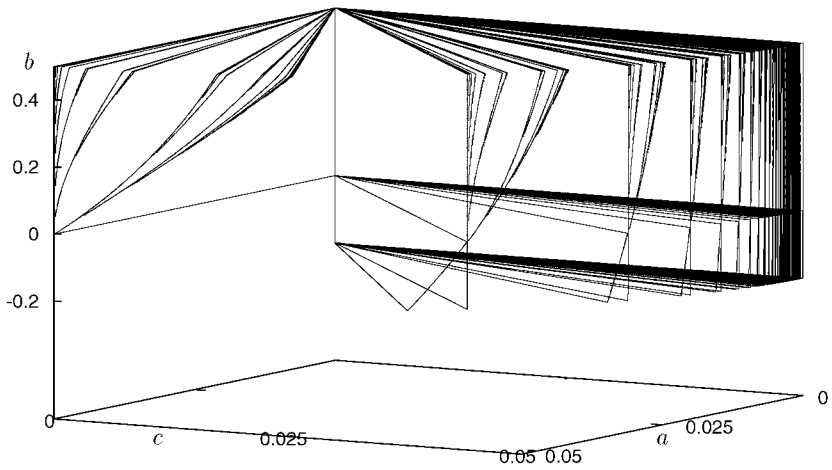

Figure 10. Structure of the 3D parameter space $[a \times b \times c]$ of the piecewise-linear map (1) in the vicinity of the origin (unfolding of the three-parametric bifurcation at the origin).

$\phi_{\min}^{\mathcal{LR}^{n-1}}$ and $\phi_{\max}^{\mathcal{LR}^{n}}$. Along each of the bifurcation lines, an infinite number of bifurcation surfaces starts, because the situation in the $[b \times \phi]$ subspace does not depend on the radius. Each point of these surfaces represents a standard one-parametric bifurcation, namely a border-collision bifurcation (see figure 7(*b*)). Note that the described situation is not specific for the investigated 1D piecewise-linear map but seems to be a frequent case, occurring by the investigation of multi-parametric parameter spaces.

8. Summary

In this paper a 1D piecewise-linear map is considered. The part of the 3D parameter space where this map shows periodic dynamics is investigated in detail. It is demonstrated that the behaviour of the investigated map is determined by border collision bifurcations, whereby the areas in the parameter space leading to specific limit cycles can be obtained analytically. The main result of the presented work is a detailed description of the multi-parametric bifurcations in the investigated piecewise-linear map. It is shown that this map shows not only the usual one-parametric bifurcations but also an infinite number of two-parametric bifurcations as well as a three-parametric bifurcation at the origin.

9. Outlook

In this paper only the part of the 3D parameter space is investigated where the considered piecewise-linear map shows periodic dynamics. However, the multi-band chaotic attractors of this map also represent a challenging object for future research. Especially the bifurcation scenarios, for instance the one presented in figure 2(*a*), have to be investigated in detail. In this context, the following idea should be pointed out: when dealing with periodic attractors of smooth dynamical systems, the period doubling represents one of the most investigated bifurcation scenarios. The periods of limit cycles are given in this case by the geometrical series $p_n = p_0 \cdot 2^n$ where p_0 is the starting period and p_n the period after the nth flip bifurcation. It is also well known that the period doubling scenario is typically followed by the band merging scenario, where the number of bands of chaotic multi-band attractors is given by the same

geometrical series (in reverse order). Remarkably, both scenarios are strongly connected (for instance, the limit cycles, becoming unstable at the nth flip bifurcation, are involved in the nth band merging bifurcation). When dealing with piecewise-smooth dynamical systems, the period increment scenario like the one presented in figures 4(b) and (c) is often observed. In this case, the periods of limit cycles are given by the arithmetical series $p_n = p_0 + n\Delta p$, with the starting period p_0 and the increment value Δp. As far as we know, the corresponding scenario, where the number of bands of chaotic multi-band attractors is described by the arithmetical series, has not been investigated until now. The phenomenon presented in figure 2(a) leads us to the assumption that this scenario exists and that there is also a connection between this scenario and the period increment scenario.

Appendix A. Proof of equation (3)

It can be easily shown that the points belonging to the limit cycle $O_{\mathcal{LR}^{n-1}}$ satisfy the condition

$$x_0 < 0 < x_{n-1} < x_{n-2} < \cdots < x_2 < x_1. \tag{A.1}$$

Because both partial functions f_l and f_r are linear with respect to x, we can calculate for all n

$$x_1 = bx_0 + c \qquad x_2 = bx_0 + c - a \qquad x_3 = bx_0 + c - 2a \tag{A.2}$$

$$\ldots$$

$$x_{n-1} = bx_0 + c - (n-2)a, \tag{A.3}$$

$$x_n = bx_0 + c - (n-1)a. \tag{A.4}$$

Then equation (3) follows directly from equation (A.4) and the periodicity condition $x_n = x_0$.

Appendix B. Proof of equation (5)

In order to prove equation (5), one has to determine the parameter values for which equation (A.1) is satisfied. Hereby it is necessary to consider only the conditions $x_0 < 0$ and $x_{n-1} > 0$. Inserting equation (3) into these conditions, one obtains equation (5).

Appendix C. Proof of equation (6)

Note that the natural measure $\rho(x)$ of an n-periodic attractor $\mathcal{A} \subset R$ is uniformly distributed on its points, i.e. is given by

$$\rho(x) = \frac{1}{n}\sum_{i=0}^{n-1}\delta(x - x_i), \qquad \text{with } x_i \in \mathcal{A}, \tag{C.1}$$

where $\delta(x)$ denotes the δ-function. Using now the well-known relation for the Lyapunov exponent for attractors of 1D maps $x_{n+1} = f(x_n)$, namely

$$\lambda(\mathcal{A}) = \int_R \rho(x)\ln\left|\frac{\mathrm{d}f(x)}{\mathrm{d}x}\right|\mathrm{d}x, \tag{C.2}$$

we obtain for the Lyapunov exponent

$$\lambda(O_{\mathcal{LR}^{n-1}}) = \int_R \frac{1}{n}\sum_{i=0}^{n-1}\delta(x - x_i)\ln\left|\frac{\mathrm{d}f(x)}{\mathrm{d}x}\right|\mathrm{d}x = \frac{1}{n}\left(\ln|b| + \sum_{i=1}^{n-1}\ln 1\right) = \frac{\ln|b|}{n} < 0. \tag{C.3}$$

Equations (12) and (14) are obtained analogously.

References

[1] Hamill D C, Deane J H B and Jefferies D J 1992 Modeling of chaotic dc–dc converters by iterated nonlinear mappings *IEEE Trans. Power Electron.* **7** 25–36

[2] Deane J H B 1992 Chaos in current-mode controlled boost dc–dc converter *IEEE Trans. Circuits Syst. I* **39** 680–3

[3] Tse C K 1994 Flip bifurcation and chaos in three-state boost switching regulators *IEEE Trans. Circuits Syst. I* **41** 16–23

[4] Fossas E and Olivar G 1996 Study of chaos in the buck converter *IEEE Trans. Circuits Syst. I* **43** 13–25

[5] di Bernardo M, Budd C J and Champneys A R 1998 Grazing, skipping and sliding: analysis of the nonsmooth dynamics of the dc/dc buck converter *Nonlinearity* **11** 858–90

[6] di Bernardo M, Garofalo F, Glielmo L and Vasca F 1998 Switchings, bifurcations and chaos in dc/dc converters *Fundam. Theory Appl.* **45** 133–41

[7] Yuan G, Banerjee S, Ott E and Yorke J A 1998 Border-collision bifurcations in the Buck converter *Fundam. Theory Appl.* **45** 707–16

[8] di Bernardo M and Vasca F 2000 Discrete-time maps for the analysis of bifurcations and chaos in dc/dc converters *IEEE Trans. Circuits Syst. I* **47** 130–43

[9] Banerjee S, Karthik M S, Yuan G and Yorke J A 2000 Bifurcations in one-dimensional piecewise smooth maps—theory and applications in switching circuits *IEEE Trans. Circuits Syst. I: Fundam. Theory Appl.* **47** 389–94

[10] Banerjee S, Ranjan P and Grebogi C 2000 Bifurcations in two-dimensional piecewise smooth maps—theory and applications in switching circuits *IEEE Trans. Circuits Syst. I: Fundam. Theory Appl.* **47** 633–43

[11] Olivar G, Fossas E and Batlle C 2000 Bifurcations and chaos in converters. Discontinuous vector fields and singular Poincaré maps *Nonlinearity* **13** 1095–121

[12] Iu H H C and Tse C K 2001 Bifurcation behavior in parallel-connected buck converters *Fundam. Theory Appl.* **48** 233–40

[13] Banerjee S and Verghese G C (ed) 2001 *Nonlinear Phenomena in Power Electronics—Attractors, Bifurcations, Chaos, and Nonlinear Control* (Piscataway, NJ: IEEE)

[14] di Bernardo M, Vasca F and Olivar G 2001 Routes to chaos in the voltage controlled buck converter without latch *Nonlinear Phenomena in Power Electronic Circuits* ed G Verghese and S Banerjee (Piscataway, NJ: IEEE)

[15] Peterka F 1974 Laws of impact motion of mechanical systems with one degree of freedom: part i. Theoretical analysis of n-multiple $(1/n)$-impact motions *Acta Tech. CSAV* **4** 462–73

[16] Peterka F 1974 Laws of impact motion of mechanical systems with one degree of freedom: part ii. Results of analogue computer modelling of the motion *Acta Tech. CSAV* **4** 569–80

[17] Shaw S W and Holmes P J 1983 A periodically forced piecewise linear oscillator *J. Sound Vib.* **90** 129–55

[18] Nordmark A B 1991 Non-periodic motion caused by grazing incidence in an impact oscillator *J. Sound Vib.* **145** 279–97

[19] Foale S 1994 Analytical determination of bifurcations in an impact oscillator *Proc. R. Soc. Lond.* A **347** 353–64

[20] Peterka F 1996 Bifurcations and transition phenomena in an impact oscillator *Chaos, Solitons Fractals* **7** 1635–47

[21] Chin W, Ott E, Nusse H E and Grebogi C 1994 Grazing bifurcations in impact oscillators *Phys. Rev.* E **50** 4427–44

[22] Luo G and Xie J 2000 Bifurcations and chaos in a system with impacts *Physica* D **148** 183–200

[23] Molenaar J, de Weger J G and van de Water W 2001 Mappings of grazing-impact oscillators *Nonlinearity* **14** 301–21

[24] Pavlovskaia E and Wiercigroch M 2001 Modeling of an impact system with a drift *Phys. Rev.* E **64** 056224

[25] Zhusubaliyev Zh T and Mosekilde E 2003 *Bifurcations and Chaos in Piecewise-Smooth Dynamical Systems* (*Nonlinear Science A* vol 44) (Singapore: World Scientific)

[26] Guckenheimer J and Williams R F 1979 Structural stability of Lorenz attractors *Publ. Math. IHES* **50** 307–20

[27] Gambaudo J-M, Procaccia I, Thomae S and Tresser Ch 1986 New universal scenarios for the onset of chaos in Lorenz-type flows *Phys. Rev. Lett.* **57** 925–28

[28] Feigin M I 1970 Doubling of the oscillation period with C-bifurcations in piecewise-continuous systems *Prikl. Math. Mekh.* **34** 861–9 (in Russian)

[29] Feigin M I 1975 On the generation of subharmonic modes in a piecewise-continuous system *Prikl. Math. Mekh.* **38** 810–8 (in Russian)

[30] Feigin M I 1978 On the structure of C–bifurcation boundaries of piecewise–continuous systems *Prikl. Math. Mekh.* **42** 820–9 (in Russian)

[31] Misiurevicz M and Kawczyński A L 1991 Periodic orbits for interval maps with sharp cusps *Physica* D **52** 191–203
[32] Nusse H E and Yorke J A 1992 Border-collision bifurcations including period two to period three bifurcation for piecewise smooth systems *Physica* D **57** 39–57
[33] Feigin M I 1994 *Forced Oscillations in Systems with Discontinuous Nonlinearities* (Moscow: Nauka) (in Russian)
[34] Nusse H E, Ott E and Yorke J A 1994 Border-collision bifurcations: an explanation for observed bifurcation phenomena *Phys. Rev.* E **49** 1073–6
[35] Nusse H E and Yorke J A 1995 Border-collision bifurcations for piecewise smooth one-dimensional map *Int. J. Bifurc. Chaos* **5** 189–207
[36] Lamba H and Budd C J 1994 Scaling of Lyapunov exponents at nonsmooth bifurcations *Phys. Rev.* E **50** 84–90
[37] Maistrenko Yu L, Maistrenko V L, Vikul S I and Chua L O 1995 Bifurcations of attracting cycles from time-delayed Chua's circuit *Int. J. Bifurc. Chaos* **5** 653–71
[38] Nordmark A B 1997 Universal limit mapping in grazing bifurcations *Phys. Rev.* E **55** 266–70
[39] Maistrenko Yu L, Maistrenko V L and Vikul S I 1998 On period-adding sequences of attracting cycles in piecewise linear maps *Chaos, Solitons Fractals* **9** 67–75
[40] Banerjee S, Yorke J and Grebogi C 1998 Robust chaos *Phys. Rev. Lett.* **80** 3049–52
[41] Banerjee S and Grebogi C 1999 Border collision bifurcation in two-dimensional piecewise smooth maps *Phys. Rev.* E **59** 4052–61
[42] di Bernardo M, Budd C J and Champneys A R 2001 Corner collision implies border-collision bifurcation *Physica* D **154** 171–94
[43] di Bernardo M, Budd C J and Champneys A R 2001 Normal form maps for grazing bifurcations in n-dimensional piecewise-smooth dynamical systems *Physica* D **160** 222–54
[44] di Bernardo M, Budd C J and Champneys A R 2001 Grazing and border-collisions in piecewise-smooth systems: a unified analytical framework *Phys. Rev. Lett.* **86** 2554–6
[45] Kowalczyk P and di Bernardo M 2001 On a novel class of bifurcations in hybrid dynamical systems *Hybrid Systems: Computation Control (LNCS 2034)* ed M D di Bebedetto and A Sangiovanni-Vincentelli (Berlin: Springer) pp 361–74
[46] Tanaka H and Ushio T 2002 Analysis of border-collision bifurcations in a flow model of a switching system *IEICE Trans. Fundam. Electron., Commun. Comput. Sci.* E **85-A** 734–9
[47] Kowalczyk P, di Bernardo M and Champneys A R 2004 Corner collision and grazing sliding: practical examples of border collision bifurcations *Chaotic Dynamics and Control of Systems and Processes in Mechanics* ed F Vestroni and G Rega (Dordrecht: Kluwer)
[48] Dankowicz H and Zhao X 2005 Local analysis of co-dimension-one and co-dimension-two grazing bifurcations in impact microactuators *Physica* D **202** 238–57
[49] di Bernardo M, Budd C, Champneys A R, Kowalczyk P, Nordmark A, Olivar G and Piiroinen P 2005 Bifurcations in nonsmooth dynamical systems *Preprint* 2005.04 Bristol Centre for Applied Nonlinear Mathematics
[50] Kowalczyk P, di Bernardo M, Champneys A R, Hogan S J, Homer M, Kuznetsov Yu A, Nordmark A and Piiroinen P 2006 Two-parameter nonsmooth bifurcations of limit cycles: classification and open problems *Int. J. Bifurc. Chaos* **16**
[51] di Bernardo M, Johansson K H and Vasca F 2000 Sliding bifurcations in piecewise smooth dynamical systems *Proc. NDES00 (Catania, Italy, June)*
[52] Hassouneh M A, Abed E H and Nusse H E 2004 Robust dangerous border-collision *Phys. Rev. Lett.* **92** 070201
[53] di Bernardo M, Budd C J, Champneys A R and Kowalczyk P 2005 *Bifurcations and Chaos in Piecewise Smooth Dynamical Systems: Theory and Applications* (New York: Springer)
[54] Takens F 1974 Applications of global analysis: forced oscillations and bifurcations *Commun. Math. Inst. Rijksuniversiteit Utrecht* **3** 1–59
[55] Arnold V I 1977 Loss of stability of autooscillations near resonances and versal deformations of equivariant vector fields *Funct. Anal. Appl.* **11** 1–10
[56] Zaks M A, Lyubimov D B and Pikovsky A S Universal scenarios of transitions to chaos via homoclinic bifurcations *Preprint 192(87)* Russian Academy of Science, Institute of Mechanics of Solid Matter, Sverdlovsk (in Russian)
[57] Lyubimov D V, Pikovsky A S and Zaks M A 1989 *Universal Scenarios of Transitions to Chaos via Homoclinic Bifurcations* (*Math. Phys. Rev.* vol 8) (London: Harwood Academic)
[58] Ghrist R and Holmes P 1994 Knotting within the gluing bifurcation *IUTAM Symposium on Nonlinearilty and Chaos in the Enginnering Dynamics* ed J Thompson and S Bishop (New York: Wiley) pp 299–315
[59] Ghrist R 2000 Resonant gluing bifurcations *Int. J. Bifurc. Chaos* **10** 2141–60
[60] Kuznetsov Y 2004 *Elements of Applied Bifurcation Theory* 3rd edn (Berlin: Springer)

[61] Kowalczyk P and di Bernardo M 2005 Two-parameter degenerate sliding bifurcations in Filippov systems *Physica* D **204** 204–29
[62] Nordmark A and Kowalczyk P 2006 A codimension-two scenario of sliding solutions in grazing–sliding bifurcations *Nonlinearity* **19** 1–26
[63] di Bernardo M, Kowalczyk P and Nordmark A 2003 Sliding bifurcations: a novel mechanism for the sudden onset of chaos in dry-friction oscillators *Preprint* 2003.16 Bristol Centre for Applied Nonlinear Mathematics
[64] Takens F 1987 Transition from periodic to strange attractors in constrained equations *Dynamical Systems and Bifurcation Theory* (*Pitman Research Notes in Mathematics Series* vol 160) ed M I Camacho *et al* (Harlow, Essex: Longman Scientific and Technical) pp 399–421
[65] Maistrenko Yu, Kapitaniak T and Szuminski P 1997 Locally and globally riddled basins in two coupled piecewise-linear maps *Phys. Rev.* E **56** 6393–9
[66] Maistrenko Yu, Sushko I and Gardini L 1998 About two mechanisms of reunion of chaotic attractors *Chaos, Solitons Fractals* **9** 1373–90
[67] Yellin E and Rabinovitch A 2003 Properties and features of asymmetric partial devil's staircases deduced from piecewise linear maps *Phys. Rev.* E **67** 016202
[68] Ostruszka A, Manderfeld Ch, Zyczkowski K and Haake F 2003 Quantization of classical maps with tunable Ruelle–Pollicott resonances *Phys. Rev.* E **68** 056201
[69] Faisst H and Eckhardt B 2003 Lifetimes of noisy repellors *Phys. Rev.* E **68** 026215
[70] Jain P and Banerjee S 2003 Border collision bifurcations in one-dimensional discontinuous maps *Int. J. Bifurc. Chaos* **13** 3341–52
[71] Ott E 1993 *Chaos in Dynamical Systems* (Cambridge: Cambridge University Press) pp 26–31
[72] Lozi R 1978 Un attracteur étrange du dype attracteur de hénon *J. Phys. (Paris)* **39** 69–77
[73] Devaney R L 1984 A piecewise linear model for the zones of instability of an area preserving map *Physica* D **10** 387–93
[74] Wiggins S 1990 *Introduction to Applied Nonlinear Dynamical Systems and Chaos* (Berlin: Springer)
[75] Dolnik M and Marek M 1991 Phase excitation curves in the model of forced excitable reaction systems *J. Phys. Chem.* **95** 7267–72
[76] Field R J and Noyes R M 1977 Mechanisms of chemical oscillators: conceptual bases *Acc. Chem. Res.* **10** 214–21
[77] Field R J and Noyes R M 1977 Mechanisms of chemical oscillators: experimental examples *Acc. Chem. Res.* **10** 273–80
[78] Nicolis G and Prigogine I 1977 *Self-Organization in Nonequilibrium Systems—From Dissipative Structures to Order through Fluctuations* (New York: Wiley)
[79] Hao B-L 1991 Symbolic dynamics and characterization of complexity *Physica* D **51** 161–76
[80] Perez J M 1985 Mechanism for global features of chaos in a driven nonlinear oscillator *Phys. Rev.* A **32** 2513–6
[81] Avrutin V and Schanz M 2000 On the scaling properties of the period-increment scenario in dynamical systems *Chaos, Solitons Fractals* **11** 1949–55
[82] Avrutin V and Schanz M 2004 Border-collision period-doubling scenario *Phys. Rev.* E **70** 026222
[83] Cvitanović P, Jensen M, Kadanoff L and Procaccia I 1985 Renormalization, unstable manifolds, and the fractal structure of mode locking *Phys. Rev. Lett.* **55** 343–6
[84] Avrutin V, Wackenhut G and Schanz M 1999 On dynamical systems with piecewise defined system functions *Proc. Int. Conf. Tools for Mathematical Modelling MATHTOOLS'99 (St Petersburg)* pp 4–20
[85] Avrutin V 2004 On behavior of dynamical systems with piecewise-smooth system function *PhD Thesis* University of Stuttgart (in German)
[86] Procaccia I, Thomae S and Tresser Ch 1987 First-return maps as a unified renormalization scheme for dynamical systems *Phys. Rev.* A **35** 1884–900